Liquid Metal/Metal Oxide Frameworks

Wei Zhang, Jian Zhen Ou, Shi-Yang Tang, Vijay Sivan, David D. Yao, Kay Latham, Khashayar Khoshmanesh, Arnan Mitchell, Anthony P. O'Mullane, and Kourosh Kalantar-zadeh**

A new platform described as the liquid metal/metal oxide (LM/MO) framework is introduced. The constituent spherical structures of these frameworks are made of micro- to nanosized liquid metal spheres and nanosized metal oxides, combining the advantages of both materials. It is shown that the diameters of the spheres and the stoichiometry of the structures can be actively controlled. Additionally, the liquid suspension of these spheres demonstrates tuneable plasmon resonances. These spherical structures are assembled to form LM/MO frameworks which are capable of demonstrating high sensitivity towards low concentrations of heavy metal ions, and enhanced solar light driven photocalalytic activities. These demonstrations imply that the LM/MO frameworks are a suitable candidate for the development of future high performance electronic and optical devices.

1. Introduction

"Solid state metal"/"metal oxide" (SM/MO) micro- and nanostructures have attracted great interest for their unique physiochemical properties, which are achieved in combination but are not exhibited by the individual metal and metal oxides counterparts.[1–4] These interesting properties originate from the functionalities of both metals and metal oxides as well as the interfaces between them, providing systems which enable the manipulation of charge, light, and mechanical vibrations as well as many other functionalities.[5–7]

A variety of solid metals have been used in forming SM/MO structures.[8–11] It has been shown that these structures facilitate charge separation, assist in light absorption and scattering as well as in providing a template for generating strong surface plasmon resonances (SPR).[12–16] They have also been used for a variety of sensing applications including chemical and biochemical sensors.[17–21]

In principle, solid metals can be replaced by liquid metals to form "liquid metal"/"metal oxides" (LM/MO) structures. Interestingly, despite their immense potentials, LM/MO structures have rarely been reported.[22] Furthermore, none of these works take advantage of the nature of the incorporated liquid metals. In addition to the well-known benefits that solid metals can offer, liquid metals add extra dimensions to the structures, which originate from their soft and liquid nature. This brings flexibility, the possibility of amalgamation with other metals and their recoverability, mobility and high conformation to the system.

We have previously shown the possibility of coating relatively large liquid metal droplets of galinstan using metal oxide nanoparticles.[23–25] By doing this, we created liquid metal marbles with extraordinary physical and chemical properties. Our investigations associated these properties to the interfaces between liquid metal and metal oxide nanoparticles in combination with the flexibility of the marbles, thereby providing extra degrees of freedom in order to manipulate their functionalities on demand. However, the properties of large liquid metal marbles are strongly surface dependent and the bulk of the droplet is mostly redundant. For using the bulk of liquid metals, it should be divided into the smallest possible stable entities.

It has been demonstrated that sonication of bulk liquid metal droplets can produce micro-, meso-, and nanosized liquid metal spheres. Previous reports show that thiol-stabilized mercury and EGaIn (75 wt% Ga, 25 wt% In) liquid metal droplets with dimensions in the order of micro- to nanometer can be successfully synthesized through sonication.[26,27]

In this work, we utilize micro- to nanosized galinstan spheres with coated metal oxide nanoparticles to form the LM/MO spherical structures suspended in aqueous solutions. Galinstan (68.5 wt% Ga, 21.5 wt% In, and 10 wt% Sn) is chosen as it poses less health hazards in comparison to liquid metals such as mercury. The surface metal oxide nanoparticles are either inherently formed during the synthesis process or coated onto the surface of galinstan spheres. We fully characterize the LM/MO spherical structures in terms of stoichiometry and optical properties, including the demonstration of plasmon

W. Zhang, Dr. J. Z. Ou, S.-Y. Tang, Dr. V. Sivan, D. D. Yao, Dr. K. Khoshmanesh, Prof. A. Mitchell, Prof. K. Kalantar-zadeh
School of Electrical and Computer Engineering
RMIT University, GPO Box 2476
Melbourne VIC 3001, Australia
E-mail: zhangweizeable@gmail.com; kourosh.kalantar@rmit.edu.au

Dr. K. Latham
School of Applied Sciences
RMIT University, GPO Box 2476
Melbourne VIC 3001, Australia

Dr. A. P. O'Mullane
School of Chemistry
Queensland University of Technology
GPO Box 2434
Brisbane QLD 4001, Australia

DOI: 10.1002/adfm.201304064

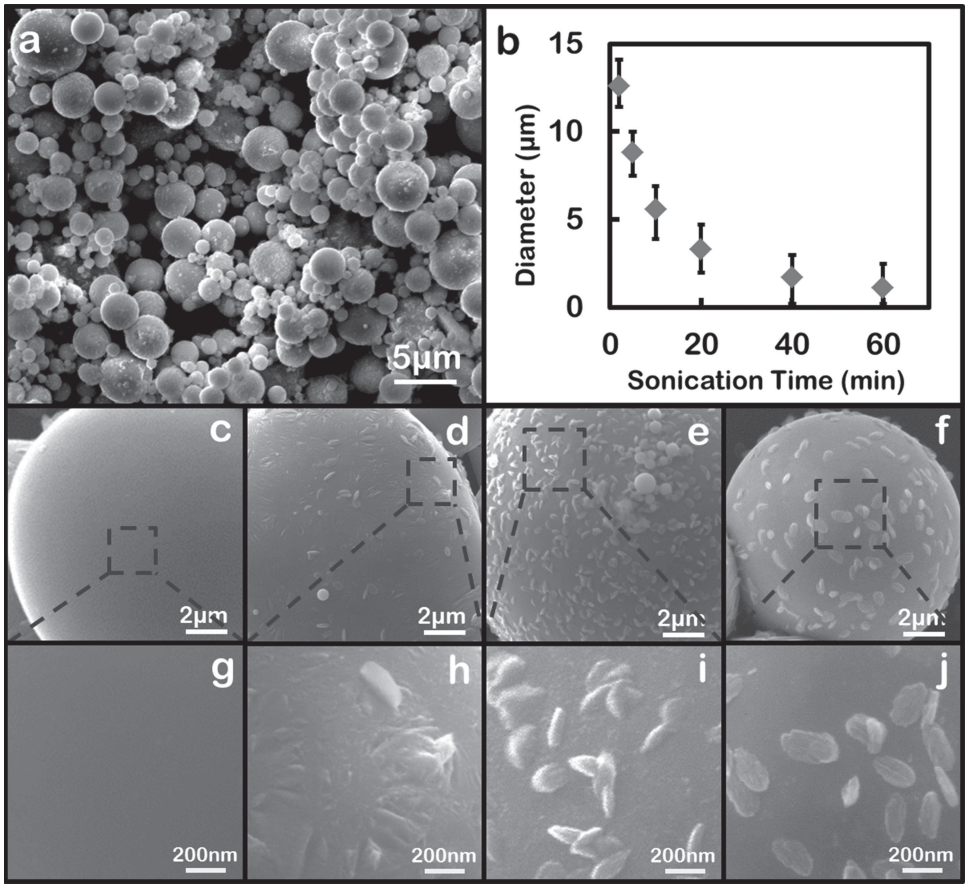

Figure 1. a) A top view SEM image of an assembly of LM/MO spherical structures after 20 min sonication. b) The plot of average diameters of spheres within spherical structures after different sonication durations. SEM images of spheres after sonication for c) 2, d) 5, e) 10, and f) 20 min and g–j) their corresponding magnified images.

resonances. To show the functionality of the created material, we assemble LM/MO spherical structures into LM/MO frameworks and investigate their capabilities as recoverable and reusable photocatalysts. In addition, we demonstrate a highly sensitive electrochemical sensor for the detection of heavy metal ions.

2. Synthesis and Characterization of LM/MO Spherical Structures

Micro- to nanosized liquid metal/metal oxide spherical structures are prepared from bulk galinstan metal (Geratherm Medical AG, Geschwenda, Germany) in the presence of sonication induced forces for different durations (Figure S1, Supporting Information). (Details are shown in Experimental Section.) The surface morphology of LM/MO spherical structures is investigated using a scanning electron microscope (SEM). **Figure 1**a is an image of an assembly of LM/MO spherical structures after sonication for 20 min. It is found that the dimensions of these spheres are related to the sonication duration. The average size of the spheres is observed to reduce from ≈13 to ≈1 μm with the increase in the sonication duration from 2 to 60 min (Figure 1b). As discussed in our previous report, galinstan droplets exposed to aqueous solutions or air are homogenously covered by a thin native oxide layer.[23] The morphology of this thin native oxide layer is also found to be strongly dependent on the sonication duration. Figure 1c–j show SEM images of LM/MO spherical structures prepared after different sonication durations of 2, 5, 10, and 20 min, respectively. From Figure 1c,g, the surface of the spheres appears smooth with no wrinkles after 2 min sonication, indicating that the native oxide layer has not been disturbed by the sonication induced forces after such a short duration. However, increasing the sonication duration to 5 min results in a winkled appearance on the surface of the spheres (Figure 1d,h). This could be caused by an increase in thickness and volume of the initial native oxide layer, which is consistent with our previous observation that the volume of metal oxide increases due to the insertion of oxygen into the metal during the oxidation process.[28] With a further increase of sonication duration to 10 min, a dense distribution of nanoplatelets can be observed on the surface of the spheres as shown in Figure 1e. These nanoplatelets have an average length and width of 200 and 50 nm, respectively (Figure 1i). After sonication for 20 min, the dimensions of these nanoplatelets increase, but concomitantly their coverage is sparser (Figure 1f,j). After 60 min of sonication, the nanoplatelets show the largest average dimensions and most of the spheres are transformed

into thicker oxide platelets (Supporting Information Figure S3). The durability of the LM/MO spherical structures in DI water is investigated and results are shown in Figure S2, Supporting Information.

Similar to galisntan, other gallium containing liquid metal alloys such as EGaIn can also be formed into LM/MO spherical structures and frameworks. As also presented in the introduction, the formation of the micro- to nano-spheres of EGaIn has been successfully demonstrated by Hohman et al.[27] Obviously, such gallium containing liquid alloys are also suitable for similar investigations. Additionally, mercury is tested for the formation of micro- to nanosized spheres under similar sonication conditions but without much success because the formed spheres are not stable and rapidly merge back into a large droplet after the sonication.

3. EDX Mapping and XPS Analysis of LM/MO Structures

The chemical composition of the observed nanoplatelets is investigated using energy-dispersive X-ray (EDX) mapping, as shown in **Figure 2**. For brevity, we only present the results for the LM/MO spherical structures after sonication for 5 and 20 min. While there is no obvious difference on the distributions of elements Ga, In, and Sn as a function of the sonication duration (Figure S6, Supporting Information), the oxygen element distribution is found to correlate with the growth of nanoplatelets on the surface of the spheres. It is identified that the oxygen element is uniformly distributed after sonication for 5 min (Figure 2e), revealing the existence of a compact but thin native oxide layer on the sphere surface after this short sonication duration. For the case of 20 min sonication, the nanoplatelets on the surface are significantly larger (Figure 2b) and their corresponding texture can be observed in the EDX mapping of the oxygen element (Figure 2f). The nanoplatelets contain significantly more oxygen than the surrounding area, confirming that they are made of galinstan oxide rather than liquid galinstan metal.

To further characterize the LM/MO spherical structures and the surface oxide nanoplatelets, we conduct X-ray photoelectron spectroscopy (XPS) measurements on LM/MO spherical structures obtained after 5 and 60 min sonication to show their composition. These two sonication durations are chosen as they represent the important points for the growth of surface oxide nanoplatelets: at 5 min, surface nanoplatelets start to emerge, while the largest dimension platelets are obtained after 60 min of sonication. In XPS spectra of Ga 3d (**Figure 3**a and b), the peak at the binding energy of 18.6 eV corresponds to metallic gallium (Ga^0),[29] whereas two peaks at 19.7 and 20.7 eV represent the valence states of Ga^{1+} in Ga_2O and Ga^{3+} in Ga_2O_3, respectively.[29] The O 2s peak at 23.9 eV is also found in the Ga 3d photoelectron spectra, which confirms the oxidation of the galinstan spheres.[30]

According to the In 3d XPS spectra shown in Figure 3c and d, the peaks locating at 443.8 and 451.4 eV are ascribed to the metallic indium (In^0).[31] Similarly, in the Sn 3d photoelectron spectra (Figure 3e,f), the peaks which are centered at 484.9 and 493.3 eV correspond to the metallic tin (Sn^0).[31] The signals reflecting the In^{3+} and Sn^{4+} states are much less significant compared to their metallic state. This means that the nanoplatelets are mainly composed of gallium oxides with a negligible amount of tin and indium oxide mixtures. Figure 3g,h shows the XPS spectra of O 1s. They can be deconvoluted into two components centered at 531.88 (marked as "L") and 533.45 eV (marked as "H"), which indicate the existence of both full stoichiometric oxides and oxygen vacancies, respectively.[32] In Figure 3g, as the area of the "H" peak is comparable to that of

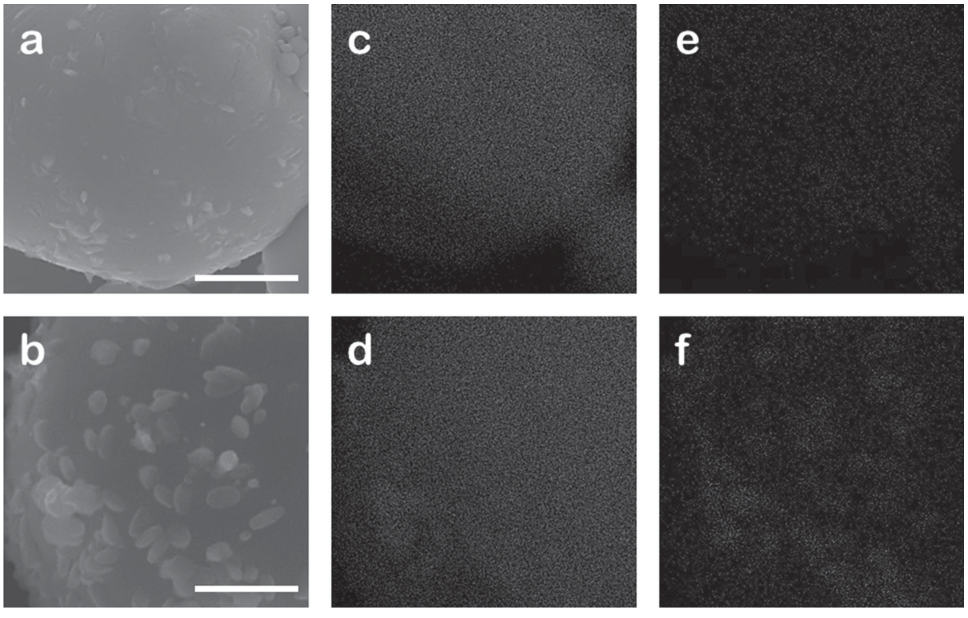

Figure 2. SEM images of LM/MO spherical structures after sonication for a) 5 and b) 20 min, respectively. Their corresponding EDX mappings of c,d) gallium element and e,f) oxygen element. All images are in the same magnification and the scale bars represent a distance of 500 nm.

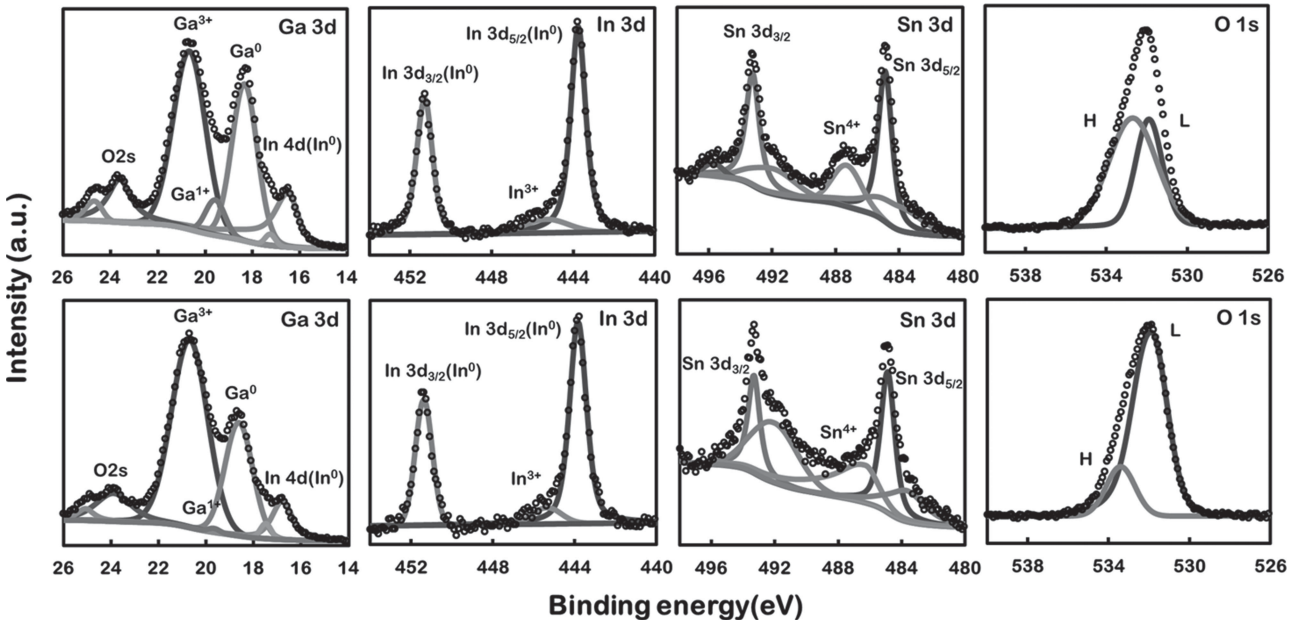

Figure 3. The XPS spectra of Ga 3d, In 3d, Sn 3d, and O 1s for LM/MO spherical structures after sonication for a,c,e,g) 5 min and b,d,f,h) 60 min.

the "L" peak, we conclude that there is a significant amount of sub-stoichiometric gallium oxide existing in the nanoplatelets.

Comparing Figure 3a,b, we find that the signals due to Ga^0 and Ga_2O significantly decrease after 60 min of sonication, which indicates the promotion of the oxidation of gallium to Ga_2O_3 by sonication. Interestingly, the signals due to metallic indium and tin are nearly constant when comparing to those after 5 min sonication. Furthermore, the intensity of "H" peaks in the oxygen spectrum presents a remarkable decrease while the intensity of the "L" peak is greatly increased, indicating the recombination of the initial oxygen vacancies during the sonication process. We believe that sonication facilitates oxidation of the galinstan surface preferentially at gallium rather than indium or tin, which is consistent with previous reports.[31,33] The stoichiometry of the whole LM/MO spherical structures is also characterized (Figure S7-A,B, Supporting Information).

4. Hypothesis of Surface Morphology Changes

Based on the aforementioned observations, we hypothesize a four phase morphological transformation process on the surface of a galinstan sphere during the sonication, which is illustrated in **Figure 4**. In phase (i) after a very short time, a thin native oxide layer is formed on the surface of the galinstan sphere. Upon prolonging the sonication duration, this oxide layer, which in time becomes thicker, is strongly deformed, wrinkled and eventually cracks under the effect of a sonication induced force (phase ii). As the oxidation reaction continues, the oxide layer is detached from the surface (phase iii) and forms small planar residues. These residual oxide layers are gradually placed on top of each other and out of registry, which is confirmed in X-ray diffraction (XRD) patterns (Figure S8, Supporting Information), appearing as randomly orientated nanoplatelets (Figure S4, Supporting Information). In phase (iv), at longer sonication times, the residual oxide nanoplatelets

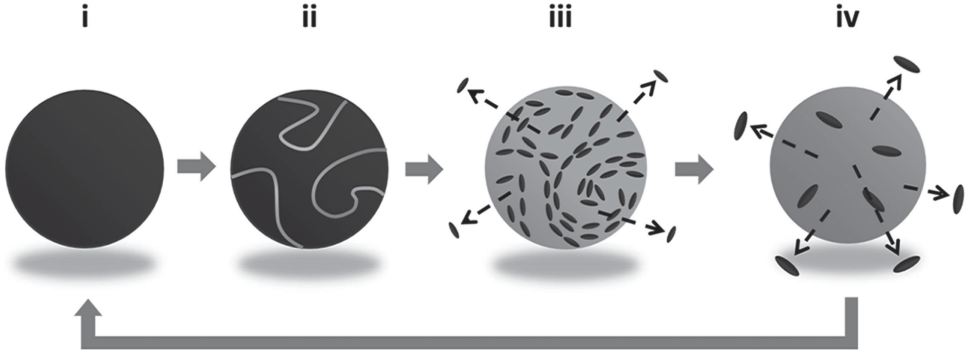

Figure 4. Schematic images of LM/MO spherical structures during sonication. Grey shapes, black shapes, and black ovals stand for galinstan spheres, oxide layers, and nanoplatelets, respectively.

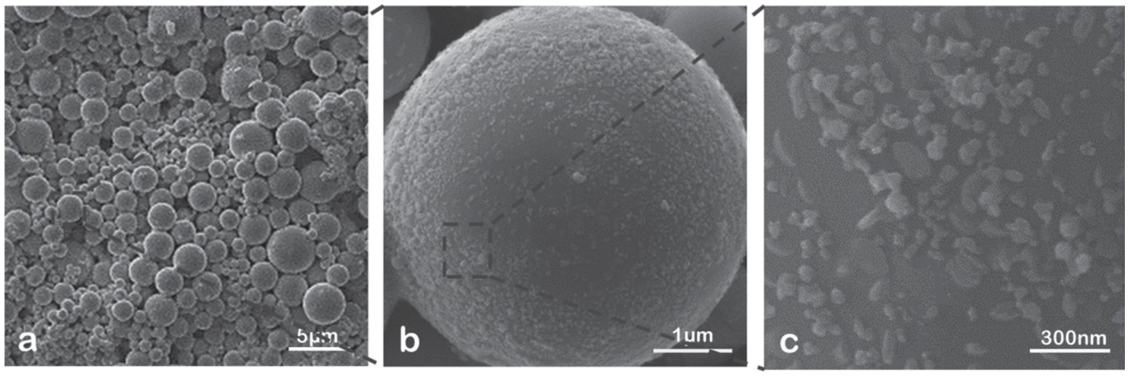

Figure 5. SEM images of an assembly of micro- and nanosized liquid metal marbles formed by coating WO_3 nanoparticles onto LM/MO spherical structures prepared after 20 min of sonication.

become thicker and are simultaneously detached, which results in larger dimension nanoplatelets but with sparser coverage on the surface of the galinstan sphere. Due to the removal of these nanoplateletes, the underlying galinstan metal is exposed to water and subsequently forms a new surface oxide layer. The newly formed oxide layer is again affected by continuous sonication and becomes thicker. Eventually, this new oxide layer will crack and form nanoplatelets. Therefore, each of these phases is continuously repeated and the galinstan sphere is gradually consumed.

5. Synthesis of Micro- and Nanosized Liquid Metal Marbles Using LM/MO Spherical Structures

As demonstrated in our previous work, liquid metal galinstan droplets can be used as a platform for the realization of liquid metal marbles.[23] Here, we demonstrate that LM/MO spherical structures can also be ultilized but with significantly smaller dimensions. By mixing galinstan spheres obtain after sonication for 20 min with metal oxide nanoparticles, we can form micro- and nanosized liquid metal marbles with a homogenous dispersion. **Figures 5** shows the surface morphology of these liquid metal marbles coated by WO_3 nanoparticles together with the nanoplatelet oxides formed during the sonication process which is previously described. The existence of WO_3 is confirmed by Raman spectroscopy as shown in Figure S9, Supporting Information. Although we only present the marbles based on the 20 min sonicated LM/MO spherical structures, it is obvious that sonication duration also plays an important role on the dimension of the liquid metal marbles. Moreover, the concentration of nanoparticles in the liquid environment is also an important factor in determining the homogeneity and density of the coating.

6. Optical Characterization of LM/MO Spherical Structures Suspensions

UV-Visible (UV-Vis) spectroscopy is implemented to assess the optical changes of the spherical suspended structures after certain sonication duration. It is known that some ultra-doped metal oxides are capable of showing plasmon resonances in the visible region and that the substoichiometry is directly associated with the doping levels of these metal oxides.[34,35] The aforementioned XPS analysis shows that the metal oxide nanoparticles on the surface of liquid metal spheres are strongly substoichiometric, and their substoichiometry can be tuned by changing the duration of the sonication.

Figure 6 shows the UV-Vis absorption spectra of LM/MO spherical structures prepared after different sonication durations. The structures which are sonicated for 5, 10, and 20 min show a strong absorption signal in the deep UV region at less than 220 nm. This increased absorption can be ascribed to the SPR of submicron- or nanosized galinstan spheres.[27] It is noted that the SPR feature almost vanishes upon increasing the sonication time to 60 min, presumably due to the near complete oxidation of the nanosized galinstan spheres. Interestingly, a broad absorption peak spanning UV and visible wavelengths could be observed for all LM/MO spherical structures obtained after different sonication durations, which can be attributed to

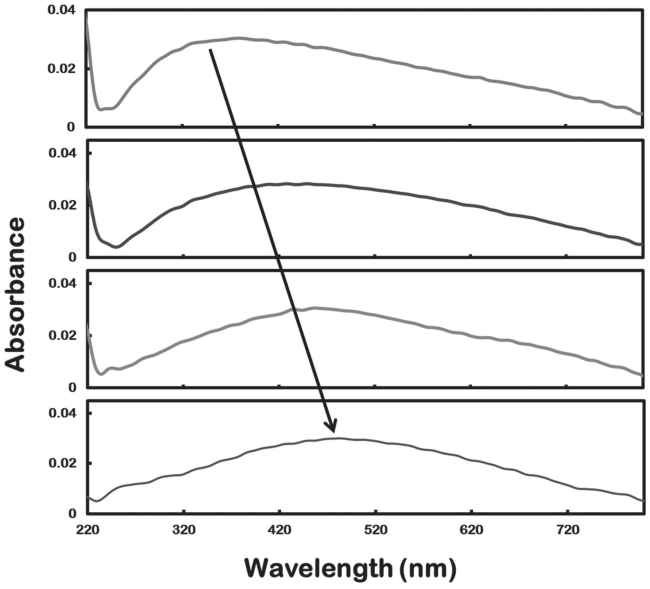

Figure 6. UV-Vis absorption spectra of the LM/MO spherical structures obtained after different sonication durations: a) 5, b) 10, c) 20, and d) 60 min.

plasmonic responses from the quasi-metallic substoichiometric gallium oxides inherently formed on the surface of the spheres. This is due to the fact that the tin and indium oxide concentrations are much less than the substoichiometric gallium oxide as evidenced by the XPS analysis. The broadness of the plasmonic peaks may be due to the polydispersity in terms of size and shape of the oxide nanostructures as evident in Figure 1. More importantly, there is a red-shift in the plasmonic peak as a result of increasing the sonication time. This shift in the plasmonic peak position is possibly due to the fact that more stoichiometric oxide is produced with increasing sonication time which causes a decrease in the oxygen vacancy concentration and hence the decrease in free charge carrier concentration.[36]

The UV-Vis spectrum of the LM/MO framework containing WO_3 nanoparticles is also measured (Figure S10, Supporting Information). Additionally, the stability of the plasmonic response of LM/MO spherical structures is investigated (Figure S11, Supporting Information). The relevant discussions can be found in the Supporting Information.

7. Heavy Metal ion Sensing and Phyotocatalytic Activities of LM/MO Frameworks

To show the functionalities of LM/MO spherical structures, they are assembled into LM/MO frameworks (the cross sectional SEM images are presented in Figure S5, Supporting Information). The preparation procedure is shown in Experimental Section. We demonstrate two different applications: heavy metal ion sensing and photocatalysis.

7.1. Heavy Metal Ion Sensing

Similar to mercury, galinstan can amalgamate with other metals and can accommodate a large concentration of different heavy metal species.[37] We have previously reported that liquid metal marbles are capable of sensing heavy metal ions with a much higher sensitivity in comparison to their liquid metal droplet counterparts without any coating.[23] We ascribe this to the generation of a localized electric field at the nanoparticle/liquid metal/electrolyte triple phase boundary as well as the large surface area produced by the nanoparticles.[23] Obviously, the LM/MO spherical structures should be able to increase the sensitivity even further as they have an impressive surface to volume ratio, which would greatly improve the effect of the nanoparticles coating, comparing to conventional liquid metal marbles.

A Pb^{2+} heavy metal ion sensing system is used to evaluate the aforementioned hypothesis. In this system, micro- and nanosized liquid metal marbles are established from coating WO_3 nanoparticles (average ≈80 nm diameter) onto LM/MO spherical structures prepared after 20 min of sonication. The micro- and nanosized liquid metal marbles are immobilized on a copper substrate and used as the working electrode, while a graphite rod and Ag/AgCl (in 3 M KCl) are employed as the counter and reference electrodes, respectively. WO_3 nanoparticles are chosen as we have previously reported that the sensitivity for heavy metal ion detection using WO_3 coated liquid metal marbles is much higher than the sensitivity of uncoated galinstan droplets,[23] which is also evident in Figure S13, Supporting Information.

Figure 7 shows the differential pulse anodic stripping voltammograms as a function of Pb^{2+} concentration in ammonium acetate buffer. In all cases a cathodic potential of –0.65 V is applied for 60 s to preconcentrate metallic lead into the LM/MO electrode. The differential pulse voltammograms (DPV) are then recorded from –0.65 to –0.15 V. The oxidation peak potential for Pb^0 stripping is found to be at –0.55 V. The amplitude of this oxidation current peak has a linear response to the Pb^0 concentrations (Inset i in Figure 7). The Pb^{2+} ions detection limit of the system is found to be 100 ppb. It should be noted that in our previous study, by using a hanging galinstan droplet electrode, the reduction of Pb^{2+} to Pb^0 has a peak current of –85 μA in response to 21 ppm Pb^{2+}. The LM/MO structures based system under identical conditions demonstrates a remarkable 80 times improvement with a current amplitude of –665.8 μA (Inset ii in Figure 7). This significant improvement may be ascribed to the dramatic enhancement of the available surface area within the assembled LM/MO frameworks that is capable of accommodating more WO_3 nanoparticles which serve as nano-facilitators to generate intense electric fields. Moreover, this in turn creates a larger surface area of the liquid metal to interact with Pb^{2+} ions which increases sensitivity. The stability of the sensing performance is investigated (Figure S12, Supporting Information). The capability of simultaneously sensing several heavy metal ions using micro- and nanosized liquid metal marbles is also shown in Figure S14 (Supporting Information).

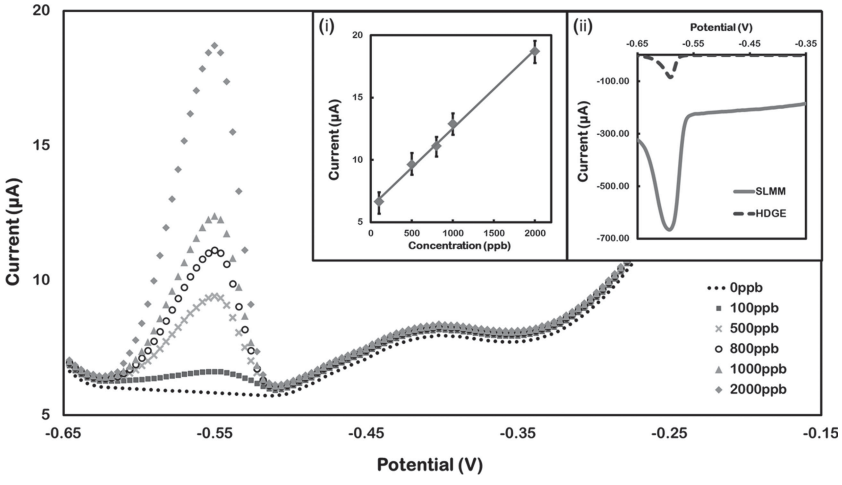

Figure 7. Differential pulse stripping voltammograms for increasing concentrations of Pb^{2+} recorded at micro- and nanosized liquid metal marbles along with the background response (solid dotted line). Inset i shows the stripping peak current values versus different concentrations of Pb^{2+}. Inset ii shows the comparison of a hanging galinstan droplet electrode (marked as "HDGE") and a micro- and nanosized liquid metal marbles (marked as "SLMM") for DPVs recorded for the reduction of Pb^{2+} to Pb^0 under same testing conditions.

There is no example for direct comparison of the heavy metal ion sensing performance of the LM/MO frameworks with their SM/MO counterparts, as none of the solid metals can efficiently amalgamate heavy metal ions, which is a unique advantage offered by liquid metals.

7.2. Photocatalytic Activities

As another demonstration of the functionality of LM/MO spherical structures, we prepare LM/MO frameworks and investigate their photocatalytic properties (preparation of these frameworks is presented in the Experimental Section). As the frameworks provide metallic/metal oxide interfaces, the photocatalytic activities should be enhanced.[38,39]

Congo red (CR) is utilized as the indicative dye to evaluate the photocatalytic performances of the LM/MO frameworks.[40] A film made of WO_3 nanoparticles, with the same weight as the films made of LM/MO frameworks, is selected as the benchmark because WO_3 is known to be one of the most efficient metal oxide photocatalysts.[41] **Figure 8**a depicts the normalized concentration of 10 μM CR in solution during simulated solar light illumination in the presence of LM/MO frameworks prepared under different sonication times and WO_3 nanoparticles only, where C_0 and C denote the concentration of CR at the start of the experiment and after certain irradiation durations, respectively.

It is noted that CR is efficiently decomposed by all four LM/MO frameworks. The highest photodegradation efficiency of 93% is observed for the LM/MO frameworks prepared after 20 min of sonication, showing the fastest photo-degradation kinetics amongst the samples. However, more importantly the frameworks consistently manifest an approximately three time enhancement in the photocatalytic activity in comparison to WO_3 nanoparticles only. This substantial improvement of the LM/MO frameworks is possibly due to the combination of the following:

1. The LM/MO spherical structures are demonstrated to have UV and visible light absorbance as presented in Figure 6. This suggests that light within a large region of the UV and visible spectra can be efficiently utilized by the frameworks.
2. The unique structure within the LM/MO frameworks, in which the galinstan oxides serve as the shell while the core remained to be galinstan metal, can be also an important factor to contribute to such an impressive improvement. It is well-known that in metal/metal oxides photocatalytic systems, the presence of the metal acts as an electron sink and suppresses electron-hole recombination and therefore promotes the hole transfer process at the semiconductor-solution interface, where organic species such as CR can be oxidized thereby realizing photocatalytic degradation.[42] Similarly, the galinstan core serves as the sink which improves interfacial charge transfer processes and charge separation.
3. Additionally, the presence of substoichiometry gallium oxide may enhance the photocatalytic activity of the system. It is known that the conduction band edges of the surface gallium oxides (which constitutes the majority of the nanoplatelets formed during the sonication process) is more negative compared to that of WO_3, resulting in a higher decomposition efficiency towards CR due to the easier transfer of valence band electrons into the conduction band which is required for a photocatalytic process.[43]

For comparison, we also include the photocatalytic properties of micro- and nanosized liquid metal marbles which are obtained by coating different weight percentages of WO_3 nanoparticles onto LM/MO spherical spheres prepared after 20 min of sonication, as shown in Figure 8b. A pristine LM/MO framework without WO_3 addition (0%) is shown as a benchmark. Interestingly, the pristine LM/MO framework displays the highest degradation efficiency. The photodegradation ability of the synthesized micro- and nanosized liquid metal marbles tends to decline upon increasing the loading of WO_3 nanoparticles, indicating that WO_3 compromises the photocatalytic efficiency of the micro- and nanosized liquid metal marbles, which is not unexpected given the poor performance of WO_3 only (Figure 8a). It appears that the intimate contact of liquid galinstan metal and the inherent nanostructured metal oxides facilitates better charge separation than that between liquid metal galinstan and the attached WO_3 nanoparticles.

The photocatalytic kinetics of our LM/MO frameworks are comparable with those of systems based on Pt nanoparticles together with WO_3 nanocrystals.[44,45] As a result, by considering that Pt is a well-known and high performance catalyst,

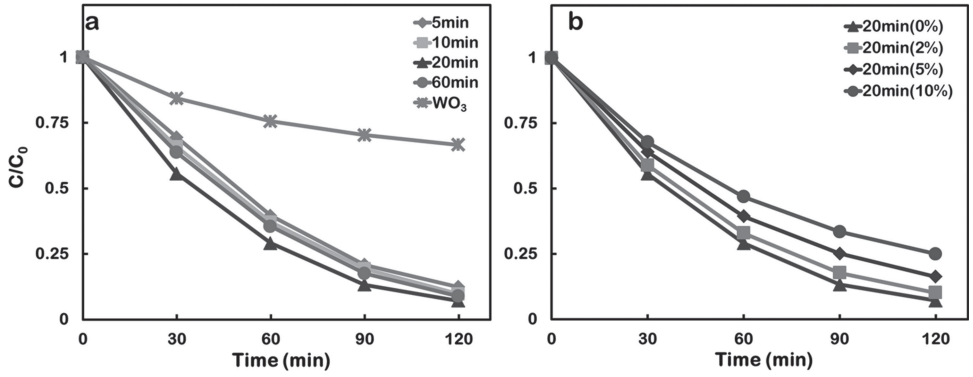

Figure 8. Photocatalytic properties of LM/MO frameworks, WO_3 nanoparticles, and micro- and nanosized liquid metal marbles. a) Degradation of 10 μM CR in the presence of LM/MO frameworks prepared after different sonication durations. WO_3 nanoparticles with the same mass serve as the benchmark. b) Degradation of 10 μM CR in the presence of micro- and nanosized liquid metal marbles containing WO_3 nanoparticles which are in different weight percentages.

our LM/MO framework is presented as a viable candidate for highly efficient photocatalysis.

The reusability of LM/MO frameworks, which is an important factor for photocatalysts, is also investigated. The photocatalytic efficiency does not show significant loss after four continuous cycles, indicating the excellent recoverability and reusability of LM/MO frameworks (Figure S15, Supporting Information). The concentrations of Ga^{3+}, In^{3+}, and Sn^{4+} ions before and after photocatalytic activities for 2 h in CR solutions are measured. The ion concentrations are within the acceptable range for human's health (Supporting Information, S16).[46]

8. Conclusion

We successfully synthesize micro- to nanosized LM/MO spherical structures, which are made of core galinstan and metal oxide nanoparticle coatings, from bulk galinstan via sonication, where the duration of the sonication is shown to be a crucial factor in influencing the morphology and stoichiometry of the oxide nanoparticles. We also demonstrate that the stoichiometry and plasmonic properties of these spherical structures in a suspension are a function of the sonication duration. We show that the visible light plasmon resonances could be actively tuned as a function of the oxygen vacancies in the spherical structures. The developed structures are assembled into LM/MO frameworks. These frameworks are then incorporated into two representative examples of heavy metal ion sensing and photocatalytic systems in order to investigate their functionalities. These spherical structures are used to form micro- and nanosized liquid metal marbles together with WO_3 nanoparticles for establishing a highly sensitive electrochemical sensing platform for heavy metal ions. These marbles are able to sense Pb^{2+} at concentrations as low as 100 ppb, indicating about 80 times improvement in comparison to the sensitivity of their bulk counterpart. This is attributed to the high surface to volume ratio of the structures as well as the formation of intense electric fields on the surface of the spheres. Furthermore, we show that these frameworks are able to provide improvement of about three times over the photocatalytic efficiency of films made of pristine WO_3 nanoparticles under similar testing conditions. This is ascribed to their excellent visible light absorption properties and the unique LM/MO interfaces that facilitate charge separation and suppression of electron-hole recombination. Good recoverability and reusability of photocatalytic LM/MO frameworks are also depicted by the results recorded during multiple cycles of the photocatalytic procedure. Altogether, the demonstrations provide strong prospects for the LM/MO structures as promising candidates for the development of other high performance devices and systems such as solar cells, photodiodes and biosensors.

9. Experimental Section

Chemicals, Reagents, and Preparation: Galinstan (Geratherm Medical AG, Geschwenda, Germany) was chosen as the source of LM/MO spherical structures and their associated liquid metal marbles. For preparation of LM/MO spherical structures suspensions, 20 µL of bulk galinstan (108.9 mg) was added into 3 mL of DI water. They were kept in a sonication bath (UNISONICS AUSTRALIA, FXP10DH, 240V ac, 5V, 50 Hz) at 25 °C for controlled durations. The samples used for UV-Vis measurements are diluted 8 times, yielding a concentration of ≈0.8 µL mL^{-1}. WO_3 nanopowder (NaBond Technologies Co., Limited, particle size ranges from 20–100 nm) was used for realizing a WO_3 suspension which was prepared by mixing 50 mg WO_3 nanopowder with 100 mL DI water to yield a concentration of 0.5 mg mL^{-1}. Then the WO_3 suspension was kept in a sonication bath for 10 min and then filtered through filter paper (Whatman Grade1) to prevent agglomeration. The micro- and nanosized liquid metal marbles were synthesized by adding different concentrations of the WO_3 suspension into the LM/MO spherical structures suspensions and then stirring for 10 min.

Characterization: A FEI Nova NanoSEM was utilized for SEM and EDX spectroscopy. For XPS measurements, a VG-310F instrument using Al non-monochromated X-rays (20 kV, 15 mA) with a hemispherical energy analyser was set at a pass energy of 100 eV for the survey spectrum and 20 eV for the peak scans. A Bruker D8 DISCOVER micro-diffractometer was used for X-ray diffraction. A system incorporating an Ocean Optics QE6500 spectrometer and a 532 nm laser was chosen to perform Raman measurements. A VARIAN 50 Bio UV-Visible spectrophotometer was used for UV-Vis spectroscopy.

Heavy Metal Ion Sensing: The micro- and nanosized liquid metal marbles suspension was synthesized by adding 10% WO_3 suspension into LM/MO spherical structures suspensions, which was obtained after sonication for 20 min. The working electrode for lead ions (Pb^{2+}) detection was first prepared by wetting copper tape with liquid galinstan. Then the liquid metal marbles suspension was uniformly deposited onto the substrate and dehydrated on a hotplate at 70 °C for 20 min. All measurements were performed using a CH Instruments (CHI 413A) electrochemical analyzer. The reference electrode was Ag/AgCl (aqueous 3 M KCl) and an inert graphite rod (3 mm diameter, Johnson Matthey Ultra "F" purity grade) was used as the auxiliary electrode. A basing three–electrode configuration was used for the electrochemical measurements. All chemicals were of analytical grade purity and all aqueous solutions were prepared using Milli–Q water. All electrochemical measurements were commenced after degassing the electrolyte solutions with nitrogen for at least 10 min prior to any measurement. For stripping voltammetry, 0.1 M acetate buffer solutions with a pH of 4.5 were used as the supporting electrolyte, which was prepared by dissolving a sample of ammonium acetate (7.7 g) from Ajax Finechem in Milli–Q water (100 mL). The pH was corrected by adding acetic acid (99.7%, Ajax Finechem) and measured using a microprocessor controlled pH meter (PH 213, HANNA Instruments). Lead ions (Pb^{2+}) were incorporated in the supporting electrolyte by dissolving lead (II) acetate 3–hydrate (BDH, AnalaR). Prior to every scan, a preconditioning step (60 s at –0.65 V) was applied. The voltammogram was recorded by applying a positive-going scan from –0.65 to 0 V (with a step increment of 5 mV, amplitude of 80 mV, and pulse period of 0.2 s). For the comparison of micro- and nanosized liquid metal marbles and hanging galinstan drop electrode, the pH value of acetate buffer solutions was adjusted to 6.0 and 33.33 g of ammonium acetate was dissolved in Milli–Q water for the buffer solution. Then all the parameters for DPV were kept constant.

Photocatalytic Activity: LM/MO structures suspensions were prepared after 5, 10, 20, and 60 min sonication. LM/MO spherical structures suspensions were uniformly deposited onto the glass substrate with a rough surface. Then the LM/MO spherical structures were dehydrated on a hotplate at 70 °C for 20 min. The WO_3 only sample was prepared using the same procedure. The deposited LM/MO spherical structures and WO_3 were of the same mass. In realization of micro- and nanosized liquid metal marbles, the WO_3 suspension was added into the LM/MO spherical structures suspensions which were sonicated for 20 min, yielding weight percentages of 0%, 2%, 5% and 10%. Then these liquid metal marbles were also dehydrated on the glass substrate using same procedure. The substrates with LM/MO frameworks were placed in the CR solution for obtaining the time-concentration charts in order to assess and compare the photocatalytic properties. All samples were put in a quartz vial containing 2 mL of 10 µM CR, which was placed 15 cm away from a simulated solar lamp (Abet Technologies

LS-150). The degradation rates of CR were determined by measuring the absorbance of the solutions at $\lambda = 500$ nm every 30 min for 120 min.

Inductively Coupled Plasma Mass Spectrometry: The concentrations of Ga^{3+}, In^{3+}, and Sn^{4+} ions in the CR solutions before and after photocatalytic activities for 2 h using an inductively coupled plasma mass spectrometer (ICP-MS) (Agilent Technologies HP4500 series 300, Shield Torch ICP-MS). The working solutions are diluted 50× with 2% nitric acid before conducting the measurements.

Supporting Information

Supporting Information is available from the Wiley Online Library or from the author.

Acknowledgements

The authors acknowledge the facilities, and the scientific and technical assistance, of the Australian Microscopy & Microanalysis Research Facility at the RMIT Microscopy & Microanalysis Facility, at RMIT University. The authors thank Paul Morrison for conducting the ICP-MS tests.

Received: December 3, 2013
Revised: February 5, 2014
Published online: March 10, 2014

[1] J. J. Yang, M. D. Pickett, X. Li, D. A. A. Ohlberg, D. R. Stewart, R. S. Williams, *Nat. Nanotechnol.* **2008**, *3*, 429.
[2] H. Hamada, *Catal. Today* **1994**, *22*, 21.
[3] P. V. Kamat, *J. Phys. Chem. Lett.* **2009**, *1*, 520.
[4] L. Novotny, N. van Hulst, *Nat. Photonics* **2011**, *5*, 83.
[5] Y.-G. Wang, Y. Yoon, V.-A. Glezakou, J. Li, R. Rousseau, *J. Am. Chem. Soc.* **2013**, *135*, 10673.
[6] X. B. Cao, L. Gu, L. J. Zhuge, W. J. Gao, W. C. Wang, S. F. Wu, *Adv. Funct. Mater.* **2006**, *16*, 896.
[7] P. X. Gao, C. S. Lao, Y. Ding, Z. L. Wang, *Adv. Funct. Mater.* **2006**, *16*, 53.
[8] K. Maeda, K. Teramura, D. Lu, N. Saito, Y. Inoue, K. Domen, *Angew. Chem. Int. Ed.* **2006**, *45*, 7806.
[9] Y. Kojima, K.-i. Suzuki, K. Fukumoto, M. Sasaki, T. Yamamoto, Y. Kawai, H. Hayashi, *Int. J. Hydrogen Energy* **2002**, *27*, 1029.
[10] C. Wang, H. Yin, S. Dai, S. Sun, *Chem. Mater.* **2010**, *22*, 3277.
[11] M. H. Yaacob, M. Breedon, K. Kalantar-Zadeh, W. Wlodarski, *Sens. Actuators B-Chem.* **2009**, *137*, 115.
[12] D. Mongin, E. Shaviv, P. Maioli, A. Crut, U. Banin, N. Del Fatti, F. Vallée, *ACS Nano* **2012**, *6*, 7034.
[13] E. Shaviv, O. Schubert, M. Alves-Santos, G. Goldoni, R. Di Felice, F. Vallée, N. Del Fatti, U. Banin, C. Sönnichsen, *ACS Nano* **2011**, *5*, 4712.
[14] S. A. Mann, E. C. Garnett, *Nano Lett.* **2013**, *13*, 3173.
[15] H. P. Paudel, M. N. Leuenberger, *Nano Lett.* **2012**, *12*, 2690.
[16] G. V. Naik, V. M. Shalaev, A. Boltasseva, *Adv. Mater.* **2013**, *25*, 3264.
[17] R. K. Joshi, S. Krishnan, M. Yoshimura, A. Kumar, *Nanoscale Res. Lett.* **2009**, *4*, 1191.
[18] E. Della Gaspera, A. Antonello, M. Guglielmi, M. L. Post, V. Bello, G. Mattei, F. Romanato, A. Martucci, *J. Mater. Chem.* **2011**, *21*, 4293.
[19] F. Hossein-Babaei, S. Rahbarpour, *Sens. Actuators B-Chem.* **2011**, *160*, 174.
[20] A. Kolmakov, M. Moskovits, *Annu. Rev. Mater. Res.* **2004**, *34*, 151.
[21] S. J. Ippolito, S. Kandasamy, K. Kalantar-zadeh, W. Wlodarski, *Sens. Actuators B-Chem.* **2005**, *108*, 154.
[22] J. Kang, J. Zhu, C. Curtis, D. Blake, G. Glatzmaier, Y.-H. Kim, S.-H. Wei, *Phys. Rev. Lett.* **2012**, *108*, 226105.
[23] V. Sivan, S.-Y. Tang, A. P. O'Mullane, P. Petersen, N. Eshtiaghi, K. Kalantar-zadeh, A. Mitchell, *Adv. Funct. Mater.* **2013**, *23*, 144.
[24] S.-Y. Tang, V. Sivan, K. Khoshmanesh, A. P. O'Mullane, X. Tang, B. Gol, N. Eshtiaghi, F. Lieder, P. Petersen, A. Mitchell, *Nanoscale* **2013**, *5*, 5949.
[25] X. Tang, S.-Y. Tang, V. Sivan, W. Zhang, A. Mitchell, K. Kalantar-zadeh, K. Khoshmanesh, *Appl. Phys. Lett.* **2013**, *103*, 174104.
[26] B. Pokroy, B. Aichmayer, A. S. Schenk, B. Haimov, S. H. Kang, P. Fratzl, J. Aizenberg, *J. Am. Chem. Soc.* **2010**, *132*, 14355.
[27] J. N. Hohman, M. Kim, G. A. Wadsworth, H. R. Bednar, J. Jiang, M. A. LeThai, P. S. Weiss, *Nano Lett.* **2011**, *11*, 5104.
[28] H. Zheng, A. Z. Sadek, M. Breedon, D. Yao, K. Latham, J. d. Plessis, K. Kalantar-zadeh, *Electrochem. Commun.* **2009**, *11*, 1308.
[29] C. C. Surdu-Bob, S. O. Saied, J. L. Sullivan, *Appl. Surf. Sci.* **2001**, *183*, 126.
[30] A. Petitmangin, B. Gallas, C. Hebert, J. Perrière, L. Binet, P. Barboux, X. Portier, *Appl. Surf. Sci.* **2013**, *278*, 153.
[31] F. Scharmann, G. Cherkashinin, V. Breternitz, C. Knedlik, G. Hartung, T. Weber, J. A. Schaefer, *Surf. Interface Anal.* **2004**, *36*, 981.
[32] M. Al-Kuhaili, S. Durrani, E. Khawaja, *Appl. Phys. Lett.* **2003**, *83*, 4533.
[33] D. Kim, P. Thissen, G. Viner, D.-W. Lee, W. Choi, Y. J. Chabal, J.-B. Lee, *ACS Appl. Mater. Interfaces* **2012**, *5*, 179.
[34] E. Kowalska, R. Abe, B. Ohtani, *Chem. Commun.* **2009**, 241.
[35] E. Kowalska, O. O. P. Mahaney, R. Abe, B. Ohtani, *Phys. Chem. Chem. Phys.* **2010**, *12*, 2344.
[36] K. Manthiram, A. P. Alivisatos, *J. Am. Chem. Soc.* **2012**, *134*, 3995.
[37] P. Surmann, H. Zeyat, *Anal. Bioanal. Chem.* **2005**, *383*, 1009.
[38] V. Subramanian, E. E. Wolf, P. V. Kamat, *Langmuir.* **2002**, *19*, 469.
[39] H. Li, Z. Bian, J. Zhu, Y. Huo, H. Li, Y. Lu, *J. Am. Chem. Soc.* **2007**, *129*, 4538.
[40] J. Z. Ou, R. A. Rani, S. Balendhran, A. S. Zoolfakar, M. R. Field, S. Zhuiykov, A. P. O'Mullane, K. Kalantar-zadeh, *Electrochem. Commun.* **2013**, *27*, 128.
[41] H. Zheng, J. Z. Ou, M. S. Strano, R. B. Kaner, A. Mitchell, K. Kalantar-zadeh, *Adv. Funct. Mater.* **2011**, *21*, 2175.
[42] A. L. Linsebigler, G. Lu, J. T. Yates, *Chem. Rev.* **1995**, *95*, 735.
[43] N. K. Shrestha, K. Lee, R. Kirchgeorg, R. Hahn, P. Schmuki, *Electrochem. Commun.* **2013**, *35*, 112.
[44] M. Miyauchi, A. Nakajima, T. Watanabe, K. Hashimoto, *Chem. Mater.* **2008**, *10*, 6258.
[45] H. Widiyandari, A. Purwanto, R. Balgis, T. Ogi, *Chem. Eng. J.* **2012**, *180*, 323.
[46] I. Moschèn, K. Schweizer, C. A. Wagner, J. Geis-Gerstorfer, F. Lang, *J. Dent. Res.* **2001**, *80*, 1753.